Am J Clin Exp Urol 2024;12(5):306-322
www.ajceu.us /ISSN:2330-1910/AJCEU0160812

Original Article

Ubiquitin C-terminal hydrolase L1 is a regulator of tumor growth and metastasis in double-negative prostate cancer

Shiqin Liu[1], Fernando Jose Garcia-Marques[2], Michelle Shen[1], Abel Bermudez[2], Sharon J Pitteri[2], Tanya Stoyanova[1,3]

[1]Department of Molecular and Medical Pharmacology, University of California, Los Angeles, Los Angeles, CA, USA; [2]Department of Radiology, Stanford University, Palo Alto, CA, USA; [3]Department of Urology, University of California, Los Angeles, Los Angeles, CA, USA

Received September 27, 2024; Accepted October 15, 2024; Epub October 15, 2024; Published October 30, 2024

Abstract: Prostate cancer is the second leading cause of cancer-related deaths among men worldwide. With heavy androgen deprivation therapies, prostate cancer may shift to androgen receptor negative and neuroendocrine negative subtype of castration resistant prostate cancer, defined as double-negative prostate cancer. Double-negative prostate cancer is associated with poor prognosis and disease mortality. The molecular mechanisms underlying the emergence of double-negative prostate cancer remain poorly understood. Here, we demonstrate that Ubiquitin C-Terminal Hydrolase L1 (UCH-L1), is negatively correlated with androgen receptor levels in prostate cancer patients. UCH-L1 plays a functional role in tumorigenesis and metastasis in double-negative prostate cancer. Knock-down of UCH-L1 decreases double-negative prostate cancer colony formation *in vitro* and tumor growth *in vivo*. Moreover, decrease of UCH-L1 significantly delays cell migration *in vitro* and spontaneous metastasis and metastatic colonization *in vivo*. Proteomic analysis revealed that mTORC1 signaling, androgen response signaling and MYC targets are the top three decreased pathways upon UCH-L1 decrease. Further, treatment with LDN-57444, a UCH-L1 small molecule inhibitor, impairs double-negative prostate cancer cell colony formation, migration *in vitro*, and metastatic colonization *in vivo*. Our study reveals that UCH-L1 is an important regulator of double-negative prostate cancer tumor growth and progression, providing a promising therapeutic target for this subtype of metastatic prostate cancer.

Keywords: UCH-L1, prostate cancer, androgen receptor, metastasis

Introduction

Prostate cancer remains the most frequently diagnosed non-cutaneous cancer type in men and the second leading cause of cancer-associated death in men [1]. Metastatic prostate cancer is often more challenging to treat and is associated with a significant decrease in survival rates and poor clinical prognosis [1-3]. Prostate cancer progression is facilitated by different molecular mechanisms, including alterations of AR signaling, genomic alterations, epigenetic modifications, metabolic reprogramming, lineage plasticity, and activation of aberrant signal pathways [3-47]. Identification of new drivers of prostate cancer tumorigenesis and progression is crucial for developing new therapeutic strategies aimed at preventing and treating metastatic prostate cancer.

The standard of care for patients presenting with metastatic prostate cancer is androgen-deprivation therapies (ADT) [48-53]. With hormone therapy, metastatic prostate cancer eventually develops treatment resistant, referred as castration resistant prostate cancer (CRPC) [46]. Metastatic CRPC can be further defined into five subtypes based on androgen receptor (AR) and neuroendocrine (NE) markers status including AR+/NE- adenocarcinoma, AR+/NE+ double-positive, AR^{low}/NE- low AR, AR-/NE- double-negative, and AR-/NE+ neuroendocrine prostate cancer (NEPC) [4, 11, 19, 54-56]. Double-negative prostate cancer presents distinct molecular and clinical features with the shortest survival rate [29, 57-61]. It was demonstrated that double-negative prostate cancer is caused by AR ablation and bypasses AR dependence by activating the

https://doi.org/10.62347/JNBR1463

MAPK/FGF pathway [57]. Nevertheless, the molecular drivers and therapeutic targets for double-negative prostate cancer remain elusive.

Ubiquitin C-Terminal Hydrolase L1 (UCH-L1) has a dual function in regulating protein stability and degradation with critical roles in regulating various cellular processes, including protein degradation and stability, apoptosis, and cell cycle regulation [62-66]. UCH-L1 can act as an oncogene as well as a tumor suppressor in cancer [67-70]. In the context of prostate cancer, UCH-L1 is silenced by promoter methylation in localized prostate cancer, while it is re-expressed and highly upregulated in 56% of NEPC [70, 71]. However, the functional role of UCH-L1 in double-negative prostate cancer remains unknown.

Here, we report that UCH-L1 expression negatively correlates with AR expression. Further, we demonstrate that UCH-L1 regulates double-negative prostate cancer growth and metastasis. Modulation of UCH-L1 decreases mTOR signaling, androgen response signaling, and MYC targets signaling which provides potential molecular mechanisms underlying UCH-L1 regulation of double-negative prostate cancer. More importantly, treatment with a UCH-L1 inhibitor, LDN-57444, decreases double-negative prostate cancer cell growth and migration *in vitro* and metastatic colonization *in vivo*. Our findings suggest that UCH-L1 is a potential molecular indicator and therapeutic target for double-negative prostate cancer.

Results

UCH-L1 regulates cell growth and tumor growth of double-negative prostate cancer in vitro and in vivo

We first analyzed the correlation of UCH-L1 mRNA levels with AR mRNA levels in published patient datasets [23, 72, 73]. Our data demonstrated that UCH-L1 mRNA levels were negatively correlates with AR mRNA levels in three independent prostate cancer cohorts (Grasso, et al.: R = -0.35, P = 0.0006; Kumar, et al.: R = -0.44, P < 0.00001, and Taylor, et al.: R = -0.28, P = 0.0013) (**Figure 1A**). These data suggest that high expression of UCH-L1 may contribute to AR loss during disease progression to AR negative prostate cancer. To test the functional role of UCH-L1 in double-negative prostate cancer, we silenced UCH-L1 in a double-negative prostate cancer cell line, DU-145, by two independent shRNAs. The knock-down efficiency of UCH-L1 was tested by Western Blot (**Figure 1B**). Downregulation of UCH-L1 in DU-145 significantly reduced colony formation ability compared to control (**Figure 1C**). Likewise, silencing UCH-L1 in DU-145 decreased subcutaneous tumor growth *in vivo* (**Figure 1D**). Decease of UCH-L1 also significantly decreased proliferation rate measured by Ki67 positive cells in the tumors (**Figure 1E**, **1F** and Supplementary Figure 1). These data suggest that UCH-L1 regulates double-negative prostate cancer cell growth and tumorigenesis *in vitro* and *in vivo*.

UCH-L1 regulates cell migration in vitro and metastasis in vivo

We next tested UCH-L1 function on double-negative prostate cancer metastasis *in vitro* and *in vivo*. Migration assay and wound healing assay revealed that knockdown of UCH-L1 in DU-145 cells significantly reduced migratory abilities *in vitro* (**Figure 2A**, **2B**). These results support a role of UCH-L1 in driving an aggressive phenotype in prostate cancer.

We further tested UCH-L1 function on metastasis using subcutaneous xenograft tumor model of spontaneous metastasis (**Figure 2C-F**). DU-145-shUCH-L1 and control (shCtl) cells were transduced with lentivirus expressing red fluorescent protein (RFP) and luciferase (Luc) for quantification and visualization of metastasis nodules. Quantification of whole-body bioluminescence signals and incidences of individual organs showed a significant decrease in DU-145-shUCH-L1-RFP-Luc group when compared to DU-145-shCtl-RFP-Luc group (**Figure 2C**, **2D**). Additionally, compared with DU-145-shCtl-RFP-Luc group, both the size and the number of the metastatic nodules of lungs displayed smaller in the UCH-L1 knockdown group (**Figure 2E**). It is notable that all DU-145-shCtl-RFP-Luc (7/7 mice) had lymph node metastasis, while only 4/7 mice of DU-145-shUCH-L1-RFP-Luc group were found metastases in lymph nodes (**Figure 2F**).

Knockdown of UCH-L1 in DU-145 cells decreases metastatic colonization in vivo

To further test the role of UCH-L1 in double-negative prostate cancer metastasis, we adopted another well-established intracardiac

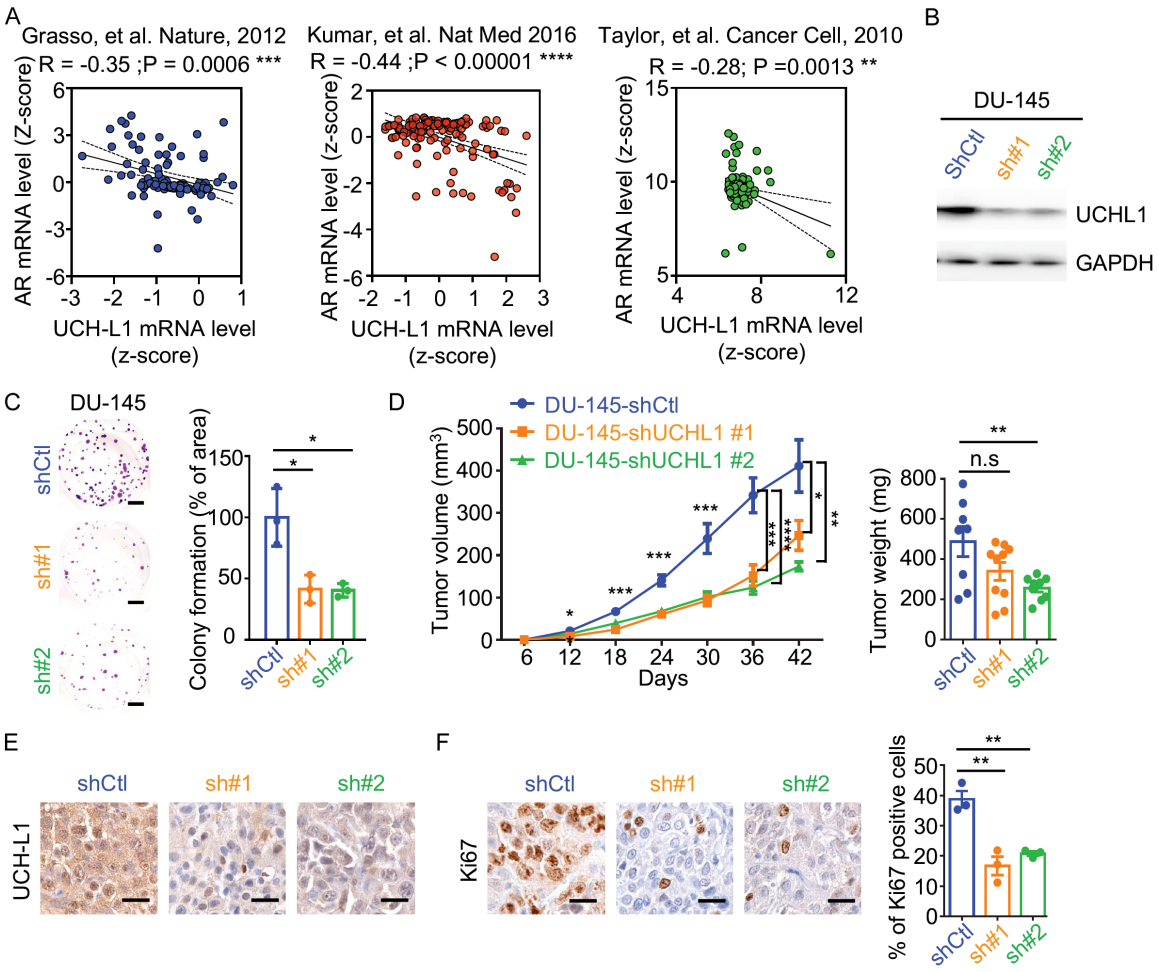

Figure 1. UCH-L1 regulates double-negative prostate cancer cell growth and tumor growth. A. mRNA levels of UCH-L1 and AR were obtained from three independent datasets. The correlation of UCH-L1 and AR mRNA levels were analyzed. R and *p* values were indicated. B. Western Blot analysis of UCH-L1 levels in DU-145-shControl (shCtl), DU-145-shUCH-L1 #1 (sh#1), and DU-145-shUCH-L1 #2 (sh#2) cells. C. Colony formation assays of DU-145-shCtl, DU-145-shUCH-L1 #1 and #2 cells. The percentage of colony area per well was quantified using ImageJ. Scale bars = 1 cm. D. Subcutaneous tumor growth of DU-145-shCtl, DU-145-shUCH-L1 #1, and #2 cells. Tumor weights at the end point were shown on the right graph. Error bars represent standard error of the mean (SEM). E, F. Immunohistochemistry (IHC) staining for UCH-L1 and Ki67 in DU-145-shCtl, DU-145-shUCH-L1 #1 and #2 xenografts. Scale bars represent 50 microns. Percentage of Ki67 positive cells of DU-145-shCtl, DU-145-shUCH-L1 #1 or DU-145-shUCH-L1 #2 tumors were quantified. Error bars represent SD. For all, *P < 0.05, **P < 0.01, ***P < 0.005, and n.s. = not significant, determined by Student's t-test (two-tailed) at each time-point.

injection metastasis model to test the role of UCH-L1 on the ability of DU-145 cells to home at distant sites (**Figure 3**) [70, 74, 75]. Similarly, bioluminescence imaging and quantification revealed that silencing of UCH-L1 in DU-145-RFP-Luc cells significantly decreased prostate cancer metastatic colonization when compared to DU-145-shCtl-RFP-Luc cells (**Figure 3A**). By quantifying red fluorescence signals in diverse organs, including liver, lungs, kidneys, and bone, we further demonstrated a remarkable decrease in the metastasis incidences, numbers, and size of metastatic nodules upon UCH-L1 knockdown in double-negative prostate cancer in comparison of the control group (**Figure 3B-F**). Importantly, bone is the most frequent metastatic site of prostate cancer, and no metastasis was found in bone from the DU-145-shUCH-L1-RFP Luc (0/8 mice) group (**Figure 3E**), suggesting knockdown of UCH-L1 diminishes metastatic colonization in double-negative prostate cancer. We confirmed that efficiency of UCH-L1 knockdown in metastatic nodules in liver, lungs, and kidneys by immuno-

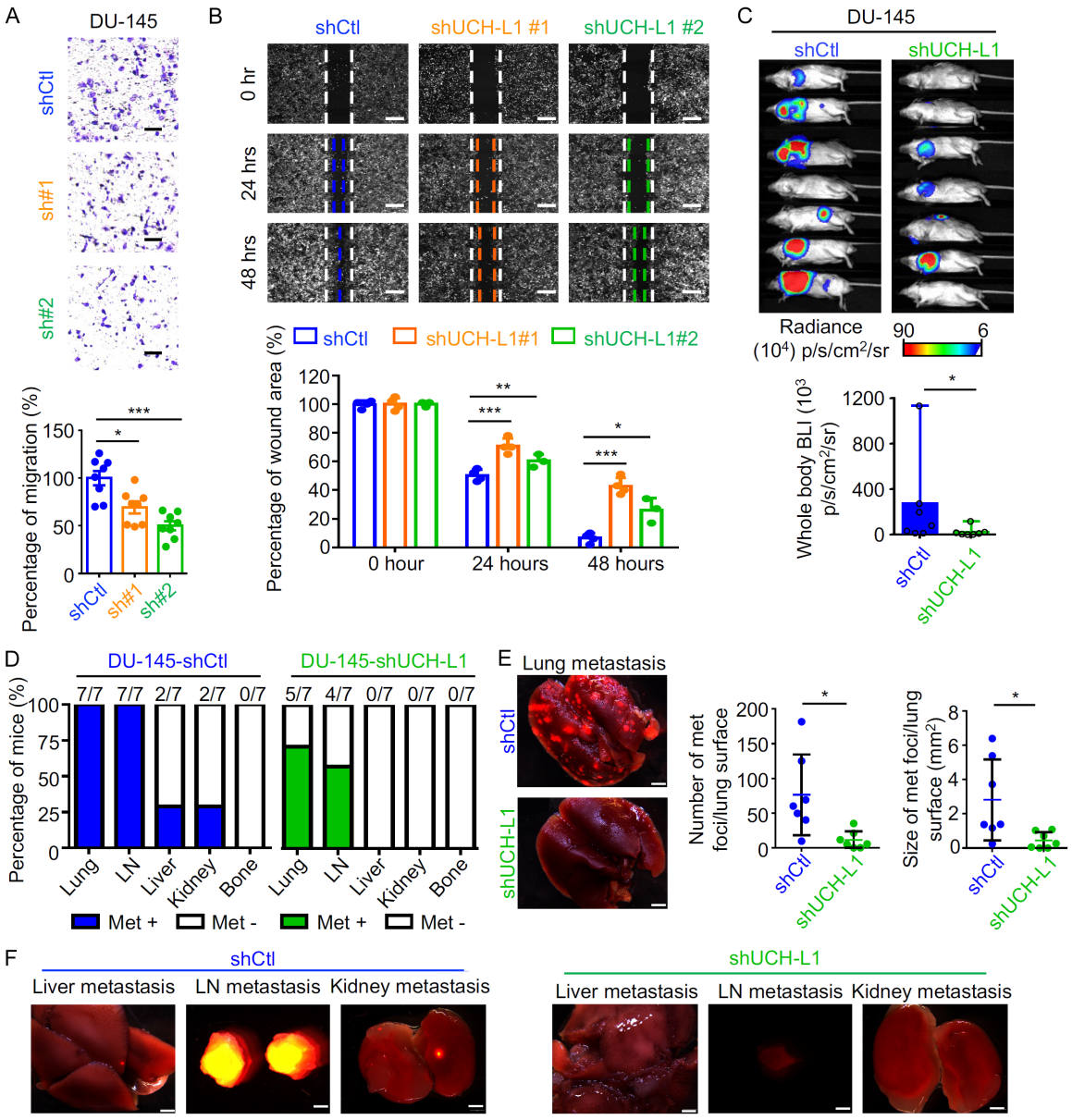

Figure 2. UCH-L1 regulates double-negative prostate cancer migration and invasion *in vitro* and *in vivo*. A. Migratory abilities of DU-145-shCtl, DU-145-shUCH-L1 #1, and DU-145-shUCH-L1 #2 cells were assessed by Transwell chamber assays. Experiments were performed in triplicate and five images per well were used for quantification. The percentage of migration were normalized to the DU-145-shCtl cell counts. Representative images of one of three independent experiments were shown. Scale bars indicate 100 microns. B. Wound healing assays of DU-145-shCtl, DU-145-shUCH-L1 #1, and DU-145-shUCHL1 #2 cells. Whole well pictures were scanned with Celigo at 0, 24, and 48 hours. The average of the wound area in three wells at 0 hour was assigned 100% and used to quantify changes in wound area over time. C. Bioluminescence imaging of DU-145-shCtl and DU-145-shUCH-L1 spontaneous model (n = 7). Whole-body bioluminescence intensity was quantified at 3 weeks post-surgery (bottom panel). D. Percentage of the mice with metastases was quantified by red fluorescence signals on each organs including lungs, lymph node (LN), liver, kidneys, and bone. E. Fluorescence images of lungs from DU-145-shCtl and DU-145-shUCH-L1. Scale bars represent 2 mm. F. RFP fluorescence images of liver, lymph node, and kidney from DU-145-shCtl and DU-145-shUCH-L1. Scale bars represent 2 mm. For all, *P < 0.05, **P < 0.01, and ***P < 0.005, determined by two-tailed Student's t test.

chemistry (IHC) staining (**Figure 3G**). Taken together, our results demonstrate that down-regulation of UCH-L1 decreases double-negative prostate cancer metastasis, suggesting

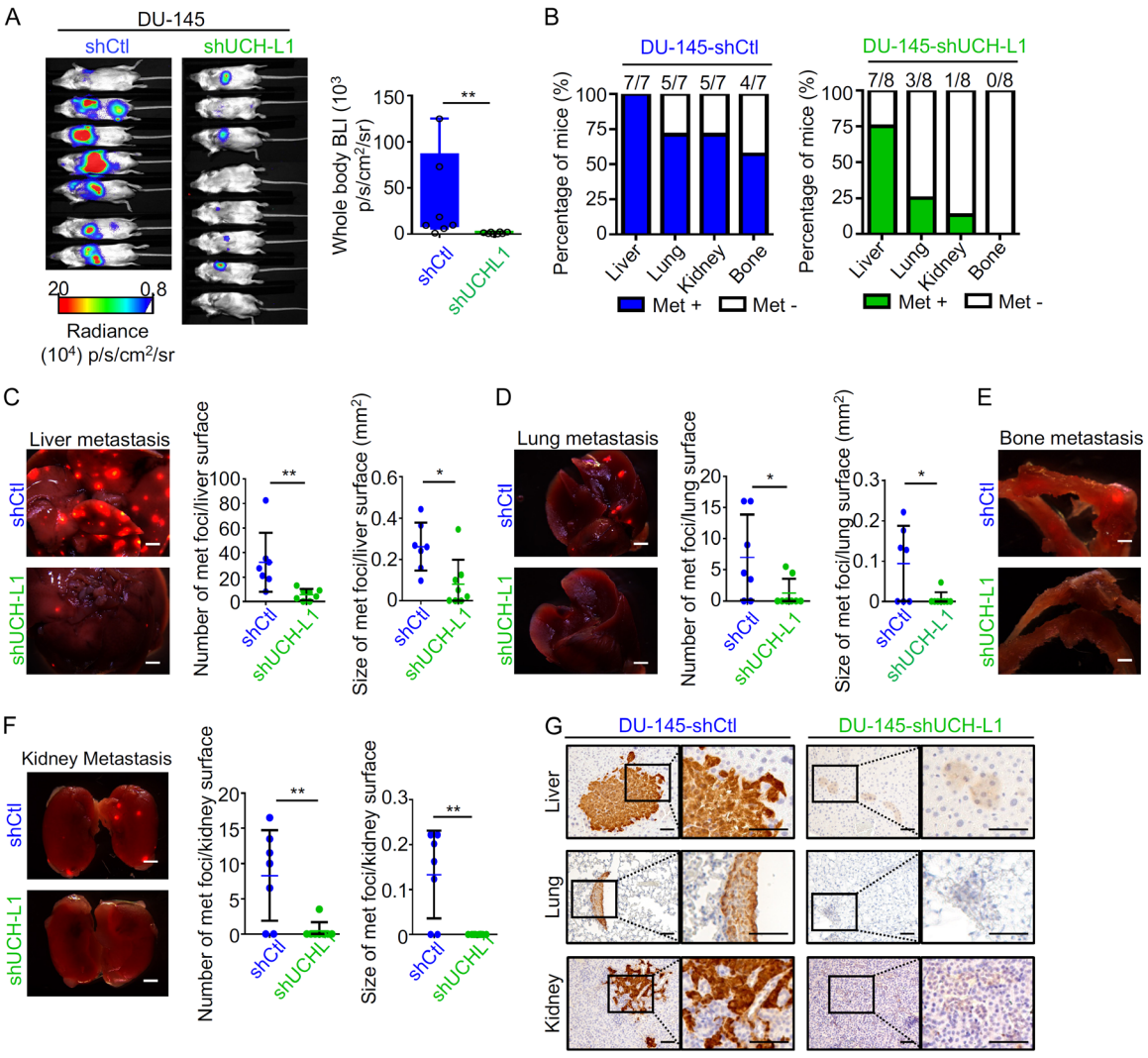

Figure 3. Downregulation of UCH-L1 decreases double-negative prostate cancer metastatic colonization. (A) DU-145-RFP-Luc-shCtl (n = 7) and DU-145-RFP-Luc-shUCH-L1 (n = 8) cells expressing luciferase and RFP were injected into the left ventricle of male NSG mice. Whole-body bioluminescence intensity (photons/second/cm^2/surface radiance) was quantified at Day 21. (B) Percentage of the mice with metastases was quantified in organs including liver, lung, kidney, and bone based on fluorescence signals. (C-F) Representative images of metastatic nodules in liver, lungs, bone, and kidneys of DU-145-shCtl and DU-145-shUCH-L1 were detected with fluorescent stereomicroscopy. Number and size of liver (C), lung (D) and kidney (F) metastases based on counting of the RFP foci using ImageJ. (G) IHC staining of UCH-L1 in liver, lung, and kidney from DU-145-shCtl and DU-145-shUCH-L1 (scale bar = 50 microns). *P < 0.05 and **P < 0.01, determined by two-tailed Student's t test.

that targeting UCH-L1 could be a potential therapeutic strategy for suppressing double-negative prostate cancer metastatic progression.

UCH-L1 regulates mTORC1 signaling, androgen response signaling, and MYC targets in double-negative prostate cancer

UCH-L1 has a dual function in regulating protein degradation and stability [76, 77]. To identify potential mechanism of how UCH-L1 regulates double-negative prostate cancer growth, we conducted proteomic analysis of two independent DU-145-UCH-L1 knockdown xenografts compared to DU-145-shCtl xenografts. 100 proteins were significantly decreased and 93 proteins were increased upon UCH-L1 knockdown when compared to control xenografts with cut off *p* value < 0.001 and fold change < -1.5 or > 1.5 (Log2) (**Figure 4A**, **4B**).

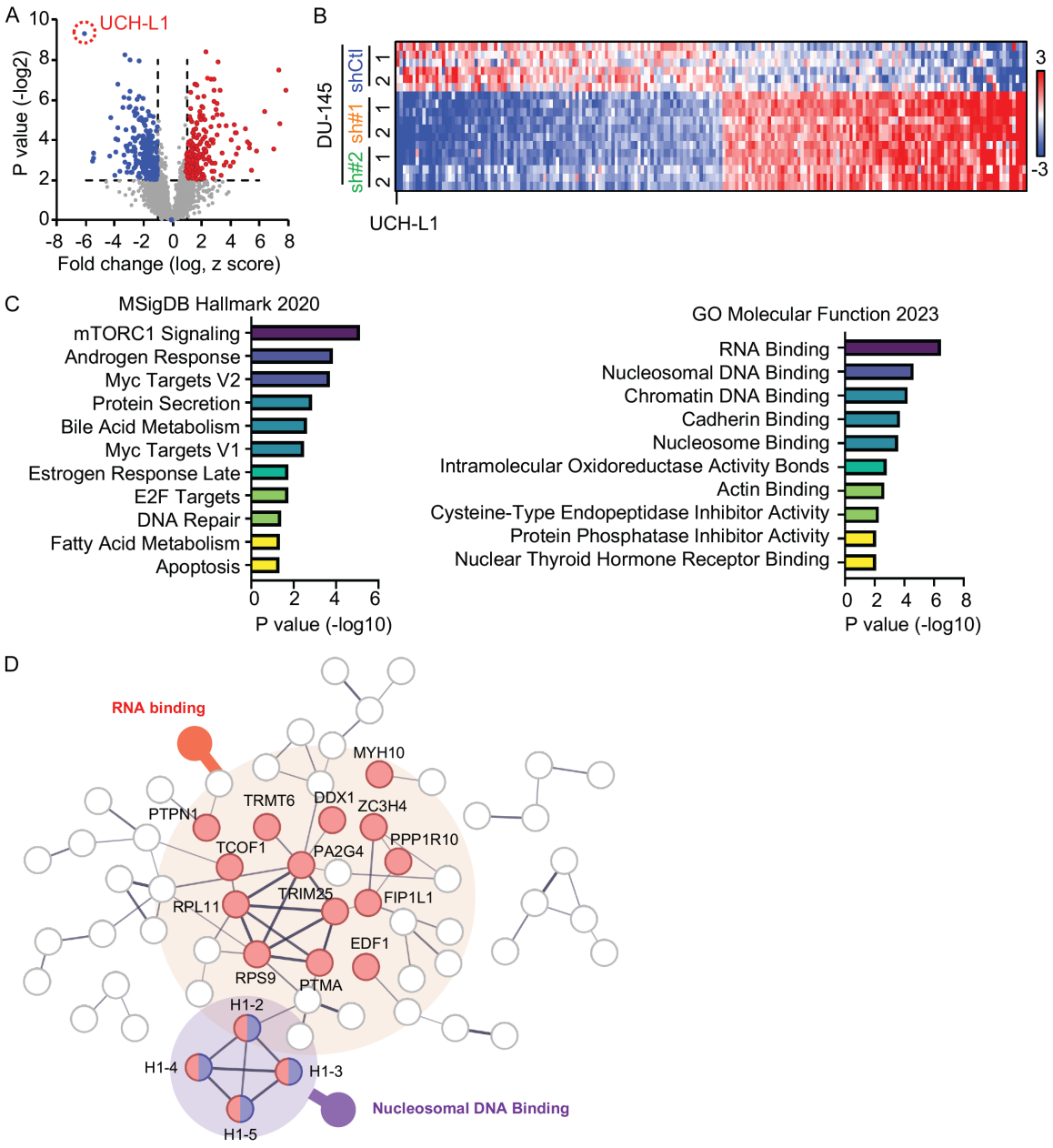

Figure 4. UCH-L1 regulates mTORC1 signaling, androgen response signaling and MYC targets in double-negative prostate cancer. A. Volcano plot of the significantly increased (red) and decreased (blue) proteins. Cut-off is based on *p* value < 0.001 and fold change > 1.5 or < -1.5 (Log2). B. Heatmap displaying fold change of the significantly increased and decreased proteins in DU-145-shUCH-L1 xenografts compared to DU-145-shCtl xenografts. C. Gene set enrichment analysis (GSEA) of decreased proteins upon UCH-L1 knockdown from MSigDB Hallmark 2020 and GO Molecular Function 2023. D. Functional protein association networks of decreased protein upon UCH-L1 knockdown in DU-145 xenografts were analyzed using STRING (https://stringdb.org/). The purple node indicates a cluster of proteins related to RNA binding. The blue node indicates a cluster of proteins related to nucleosomal DNA binding. Line thickness indicates the strength of data that support the correlation between each node.

Pathway analysis demonstrated that mTORC1 signaling, androgen response, and MYC targets signaling were the top three decreased pathways in DU-145-shUCH-L1 xenografts when compared to control xenografts (**Figure 4C**). Knockdown of UCH-L1 decreases molecular functional pathways associated with RNA binding and nucleosomal DNA binding (**Figure 4C**,

4D). Our results provide potential molecular mechanisms underlying UCH-L1 modulates double-negative prostate cancer tumor growth and metastasis.

Inhibition of UCH-L1 decreases cell growth, migration, invasion, and metastatic colonization

Lastly, we tested the therapeutic effect of UCH-L1 inhibition on double-negative prostate cancer cell growth, migration, and invasion *in vitro* and metastatic colonization *in vivo*. Treatment with UCH-L1 inhibitor, LDN-57444, significantly decreased cell growth and reduced migration and invasion abilities measured by colony formation, transwell migration, and invasion chamber assays (**Figure 5A-C**). Based on these findings, we further tested UCH-L1 inhibition on metastasis accessed by intracardiac injection model. Although no significant reduction of whole-body bioluminescence signals was found in LDN-57444 treated group compared to vehicle group in DU-145-RFP-Luc model (**Figure 5D**, **5E**), we observed a significant decrease in lung metastasis incidences (3/10 mice) when compared to vehicle group (8/8 mice) (**Figure 5E**). By quantifying the red fluorescence signals, we observed less numbers of metastases in lungs and liver from LDN-57444 treated group relative to vehicle group (**Figure 5F**). Altogether, our results demonstrate that UCH-L1 inhibition could be a potent therapeutic strategy for targeting double-negative prostate cancer progression.

Discussion

Double-negative prostate cancer, defined by AR negative and NE negative, accounts for 21-25% of castration resistant prostate cancer and is associated with worst clinical outcome in prostate cancer [29, 54, 57, 78]. Understanding the molecular mechanisms underlying double-negative prostate cancer initiation and progression is essential for the development of effective and molecular based targeted therapy for this lethal disease. Previous studies demonstrated that activation of FGFR and MAPK signaling pathways promotes double-negative prostate cancer growth which is independent of AR activity [57, 79]. Another study demonstrated that PRC1 is highly expressed in double-negative prostate cancer specifically and regulates double-negative prostate cancer stemness and immune suppression [80]. A combination of targeting PRC1 with immunotherapy serves as a potent therapeutic strategy for double-negative prostate cancer [80]. PRRX2, a target of the TGF-β pathway, was also identified as a key regulator in double-negative prostate cancer by CRISPR activation screening [81]. The PRRX2 gene signature can stratify the double-negative prostate cancer population and is associated with poor clinical outcomes [81]. Based on histologically characterizing of double-negative prostate cancer models, LuCaP PDX models, double-negative prostate cancer presents with features of squamous cell carcinoma [54].

UCH-L1 is crucial for the progression and metastasis of multiple cancer types including lymphoma, breast cancer, and neuroendocrine carcinomas [69, 70, 82, 83]. Our study suggests that the mechanisms underlying the role of UCH-L1 in double-negative prostate cancer may involve alterations in protein stability and signaling pathways that are involved in mTOR signaling, androgen response signaling, and MYC targets. Our study identifies a new key regulator for double-negative prostate cancer, suggesting that UCH-L1 is a novel therapeutic target for this lethal disease. With limited therapeutic benefit observed with LDN-57444, future study can test a new UCH-L1 specific inhibitor, IMP-1710 [84], on double-negative prostate cancer tumor growth and metastasis.

Collectively, we demonstrate that UCH-L1 mRNA levels are negatively associated with AR mRNA levels in prostate cancer patient cohorts which provides clinical evidence of the importance of UCH-L1 in AR-low or AR-negative prostate cancer. Our study demonstrates that silencing of UCH-L1 decreases double-negative prostate cancer cell growth, migration, and invasion *in vitro*, and spontaneous metastasis and colonization at distant sites *in vivo*. Moreover, inhibition of UCH-L1 decreases cell growth, migration, and metastatic colonization in double-negative prostate cancer. Our study demonstrates that UCH-L1 could be a key regulator of double-negative prostate cancer tumorigenesis and progression, which provides a potential therapeutic target for metastatic prostate cancer.

Targeting UCH-L1 expression and activity could offer a novel therapeutic approach for

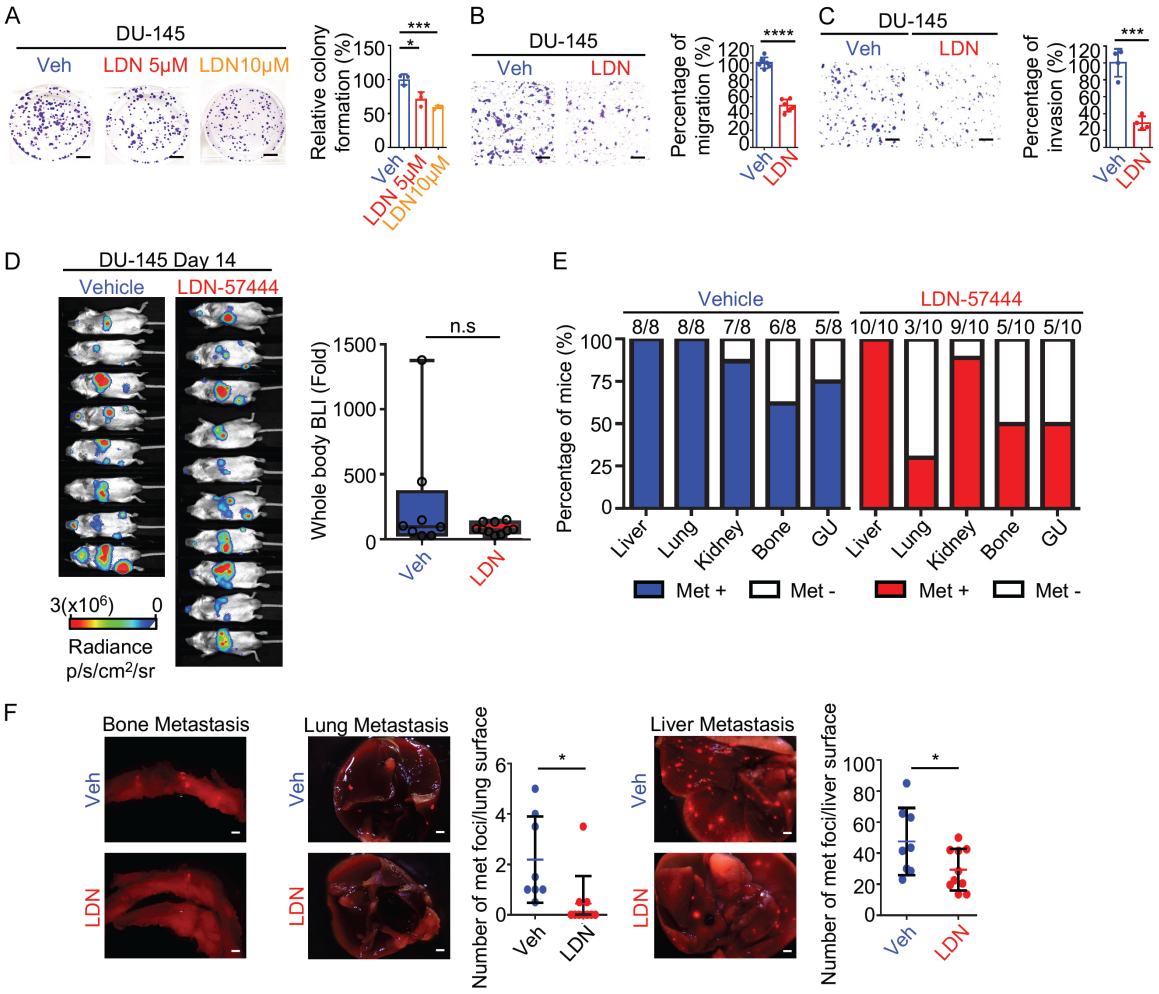

Figure 5. Inhibition of UCH-L1 decreases colony formation, migration, and invasion *in vitro* and *in vivo*. A. Colony formation assays of DU-145 cells treated with LDN-57444 (0, 5, and 10 uM). The percentage of colony area per well was quantified using ImageJ and was plotted as percentage of colony formation relative to vehicle group. Scale bars = 1 cm. B. Transwell chamber assays of DU-145 cells treated with LDN-57444 (2.5 uM) or vehicle. Scale bars = 100 microns. C. Invasion assay of DU-145 cells treated with LDN-57444 (2.5 uM) or vehicle. Scale bars represent 100 microns. D. Bioluminescence imaging of intracardiac injection metastasis model of the DU-145-RFP-Luc cells treated with LDN-57444 (5 mg/kg, corn oil, i.p., daily) or vehicle on day 14 post-treatment. The bioluminescence signal was quantified by fold change compared with day 0. E. Percentage and number of metastasis-positive animals/total animal number by organ site. F. Representative fluorescence images of metastasis organs including bone, lung, and liver. The number of metastasis nodules were quantified based on red fluorescence signals in lungs and liver (right panel). Scale bar = 2 mm. For all, *P < 0.05, and n.s. = not significant, determined by Student's t-test.

the treatment of double-negative prostate cancer.

Materials/subjects and methods

Clinical datasets

All mRNA levels were obtained from datasets on cBioPortal (www.cbioportal.org/). UCH-L1 mRNA z-score and AR mRNA z-score were obtained and analyzed from Grasso, et al. Nature, 2012; Kumar, et al. Nat Med 2016; and Taylor, et al. Cancer Cell, 2010 [23, 72, 73]. The correlation of UCH-L1 and AR mRNA levels were calculated by Prism 10.

Cell line and cell culture

DU-145 cells were purchased from the American Type Culture Collection (Cat#HTB-81, ATCC; Manassas, VA). All cells were maintained in RPMI medium supplemented with 10% FBS, 4 mM L-glutamine, and 1% penicillin/streptomycin.

Generation of control and knock-down cell lines

FUCRW lentiviral plasmid was a kind gift from Dr. Owen Witte's laboratory at University of California, Los Angeles. The pHIV-LucZsGreen plasmid is from Addgene (gift from Bryan Welm, Addgene plasmid # 39196; http://n2t.net/addgene:39196; RRID: Addgene_39196). The DU-145 cells expressing luciferase and red fluorescent protein (RFP) were generated as described previously [74]. DU-145-RFP-Luc were infected with lentiviruses carrying shControl (shCtl) RNA and two independent UCH-L1 shRNAs. The control shRNA is from Addgene (gift from David Sabatini, Addgene plasmid # 1864; http://n2t.net/addgene:1864; RRID: Addgene_1864) (CCTAAGGTTAAGTCGCCCTCGC TCGAGCGAGGGCGACTTAACCTTAGG). Validated small hairpin RNA targeting UCHL1 sequences were purchased from Millipore Sigma (St. Louis, MO). shUCH-L1 #1: TRCN0000007274; Sequence: 5'CCGGCGGGTAGATGACAAGGTGAA TCTCGAGATTCACCTTGTCATCTACCCGTTTTT-3'; shUCH-L1 #2: TRCN0000007276; Sequence: 5'CCGGCCAGCATGAGAACTTCAGGAACTCGAGTT CCTGAAGTTCTCATGCTGGTTTTT-3'. Cells were selected in puromycin (0.5 μg/mL) for 9 days.

Colony formation assay

For generation of knockdown cells, five hundred DU-145 (shCtl, shUCH-L1#1, shUCH-L1#2) cells were plated per well in 6-well plates. Colonies were cultured for nine days with medium was refreshed every third day. For drug treatment, 5×10^2 DU-145 cells were seeded per well in 6-well plates. The cells were treated with vehicle or LDN-57444 (5 or 10 uM) for nine days and the medium with compound was refreshed every three days. After nine days, colonies were fixed with ice cold methanol for 30 minutes and stained with 0.01% crystal violet for 20 minutes. Plates were scanned and quantified based on the percentage of colony-covered area per well. All experiments were performed in triplicate with three biologic replicates, and presented as mean ± SD.

Migration and invasion assay

For knocking down cells, 5×10^4 DU-145-shCtl, shUCH-L1#1, or shUCH-L1#2 cells were seeded in 300 uL serum-free medium in 24-well transwell inserts (Transwell™ Permeable Polyester Membrane Inserts). The inserts were incubated in 800 uL medium with 10% FBS in 24-well plates for 22 hours. For drug treatment, DU-145 cells were pre-treated with LDN-57444 (2.5 uM) or vehicle for 48 hours. Pre-treated DU-145 cells (5×10^4) were seeded in 300 uL serum-free medium with or without LDN-57444 (2.5 uM) in 24-well transwell inserts (migration assay) or Matrigel-coated Boyden chamber PET membrane (invasion assay). The inserts were incubated in 800 uL medium with 10% FBS and with or without LDN-57444 (2.5 uM) in 24-well plates for 22 hours. The cells that migrated or invaded the membrane to the bottom were fixed and stained with 0.01% crystal violet and manually counted. Migrated or invaded cells were normalized based on controls (shCtl or vehicle) and the percentage of migration and invasion were calculated. All experiments were performed in triplicate with three biological replicates, and presented as mean ± SD.

Wound healing assay

DU-145-shCtl, shUCH-L1#1, or shUCH-L1#2 (5×10^6) cells were seeded into 6-well plates. After cells attached and achieved full confluency, one linear scratch per well was generated using a 200 ul pipette tip. The plates were scanned by Celigo at 0, 24, and 48 hours after scratch, and migrative area was quantified at 24- and 48-hour using ImageJ software. All experiments were performed in triplicate with three biological replicates and presented as mean ± SD.

Western blot

DU-145-shCtl, shUCH-L1#1, or shUCH-L1#2 cells were collected by cell scraper and centrifuged at 500 g for three minutes. The cells were lysed in RIPA buffer with protease and phosphatase inhibitors (1:100, Thermo Fisher Scientific) for 30 mins. 40 ug proteins from DU-145-shCtl, shUCH-L1#1, or shUCH-L1#2 cells were loaded in each well of 8-16% SDS-PAGE gel (Invitrogen™ XP08165BOX) and transferred onto a 0.22 um nitrocellulose membrane (GVS Life Sciences, 1212632). Membrane was blocked with 5% non-fat milk at room temperature for 1 hour and incubated with primary antibody (Santa Cruz Biotechnology-anti-UCH-L1 (1:1000) sc-271639 or anti-GAPDH (1:1000) sc-47724) overnight at 4°C. Then the mem-

brane was washed three times with PBS-T (0.1% Tween 20) and incubated with HRP conjugated mouse secondary antibodies (1:5000, Fisher Scientific, PI31432) and developed with ECL Western Blotting Substrate (Thermo Fisher Scientific).

Immunohistochemistry

FFPE tissue sections were incubated at 65°C for 60 minutes and rehydrated in degrading percentage of ethanol. For H&E staining, slides were stained with hematoxylin for 1 minute and eosin for one minute. For immunohistochemical staining, tissue slides were steamed in 10 mM citrate buffer (pH = 6.0) at 95°C for 30 minutes. Slices were then incubated with 3% hydrogen peroxide for 5 minutes. After three times washing with water, tissue sections were blocked with 2.5% goat serum at room temperature for 1 hour. Slices were incubated with primary antibodies (anti-UCH-L1, sc-271639, 1:100; anti-Ki67, sc-23900, 1:100, Santa Cruz Biotechnology) at 4°C overnight. After three times of washing with PBS, slides were incubated with ImmPRESS® HRP secondary Antibody (MP-7452-50, Vector Laboratories) at room temperature for one hour and developed with DAB kit (Dako).

Animal models

All animal experimental procedures were approved by University of California, Los Angeles, on Laboratory Animal Care (APLAC), IACUC and all animal experiments were conducted in accordance with the Animal Ethics Committee at University of California, Los Angeles. 6-8-week-old male NSG (NOD-SCID-IL2Rγ-null) mice (Jackson Laboratory) were used in this study. Mice were housed at 65-75°F with 40-60% humidity at animal facility with veterinary care provided by the Division of Laboratory Animal Medicine at University of California, Los Angeles.

Subcutaneous xenograft model

DU-145-shCtl, shUCH-L1#1, or shUCH-L1#2 (1×10^6) cells were mixed with 80% of Matrigel in medium. Cells were subcutaneously implanted into dorsal flanks of male NSG mice. Tumor volumes were measured every six days and calculated by the equation (length × width × height)/2. At day 42 after cell implantation, subcutaneous tumors were harvested and weighed at the end point. Tumors were fixed in 10% formalin and processed and embedded in paraffin or histological analysis.

Spontaneous metastasis model

Male NSG mice were injected subcutaneously with DU-145-RFP-Luc cells expressing either shUCH-L1 or control shRNA (shCtl) on the right dorse flank. Tumor volumes were measured every six days. When tumor volumes of shCtl group reached 400 mm^3, tumors from both groups were removed by surgery. Mice were monitored by bioluminescence imaging after surgery, followed by once-a-week post-surgery for three weeks. After three weeks, organs including lungs, liver, kidneys, bones, and lymph nodes were harvested from mice after euthanizing. Organs were fixed in 10% formalin and stored in 70% ethanol for fluorescence imaging. Organs were imaged by fluorescence microscope (Stereo microscopes, Leica, Cat#M205) under red fluorescence channel and brightfield channel. The metastasis in diverse organs were quantified by red fluorescence signals.

Intracardiac injection model

For UCH-L1 knockdown cell lines, DU-145-RFP-Luc-shCtl or DU-145-RFP-Luc-shUCH-L1 cells (1×10^5 per mouse) were injected into the left ventricle of the heart of 8-weeks-old NSG male mice. Diverse organs including lungs, liver, kidneys, and bones were harvested at Day 21 post-injection. For drug treatment, DU-145-RFP-Luc (1×10^5 per mouse) were injected into left ventricle of the heart of 8-weeks-old-NSG male mice. Mice were randomized into two groups based on bioluminescence signals at day 3 post injection into two groups and treated with vehicle or LDN-57444 (5 mg/kg, corn oil, i.p., daily) for 14 days. Organs including lungs, liver, kidneys, and bones were harvested at Day 14. All organs were fixed in 10% formalin overnight and stored in 70% ethanol for histopathologic assessment. Metastatic nodules were quantified by quantitative fluorescence images.

LC-MS/MS analysis

Proteomics analysis was on 25 μg of extracted protein from each sample - flash-frozen DU-145

shControl and shUCHL1 xenografts (n = 2 per control condition, and n = 4 per shUCHL1 condition). The flash-frozen xenograft tissues were homogenized in 500 µL lysis buffer consisting of 2% sodium dodecyl sulfate (Fisher Scientific) and 1X protease inhibitor (Sigma Aldrich) using a PRO-250 (ProScientific) homogenizer probe followed by sonication. The insoluble fraction was pelleted by centrifuging the xenograft lysates at 14,000 g for 10 minutes at 4°C. Extracted protein was quantified using a bicinchoninic acid (BCA) protein assay (Thermo Fisher Scientific). Proteins were reduced with a final concentration of 10 mM Tris(2-carboxyethyl) phosphine (Sigma Aldrich) and incubated at room temperature for 1 hour. The free thiol groups were alkylated by adding iodoacetamide (Acros Organics) at a 1.5-fold molar excess of Tris(2-carboxyethyl) phosphine and incubated for 45 minutes at room temperature in the dark. Samples were digested at 37°C overnight with 1 µg sequencing grade modified trypsin enzyme (Thermo Fisher Scientific). Subsequently tryptic peptides were dried on a speed vacuum and reconstituted in 50 µl of 0.1% formic acid (Fisher Scientific) in HPLC grade water (Fisher Scientific) for LC/MS analysis. Tryptic peptides (2 µg) were loaded onto an Acclaim PepMap C18 trap column (Thermo Fisher Scientific) coupled to a Dionex Ultimate Rapid Separation Liquid Chromatography system (Thermo Fisher Scientific) at a rate of 5 µl/min for 10 minutes. A reverse-phased liquid chromatography gradient was used to separate the tryptic peptide on a 25 cm C18 analytical column (New Objective) packed in-house with Magic C18 AQ resin (Michrom Bioresources). The chromatographic program consisted on setting the flow rate to 0.5 µL/min throughout the gradient and changing the mixture of mobile phase A (0.1% formic acid in water) and mobile phase B (0.1% formic acid in acetonitrile) as follows: Mobile phase B was held at 2% B for 10 minutes with a gradual increase to 35% B for the next 110 minutes followed by a rapid increase to 85% B over 5 minutes, and ending with a 10-minute hold with 2% mobile phase B for column equilibration. Eluting peptides were directly ionized with 2.0 kV on a nanospray Flex Ion ESI source coupled to a LTQ-Orbitrap Elite mass spectrometer (Thermo Fisher Scientific). Each biological sample was analyzed in triplicate. The top ten most abundant ions per MS1 scan were selected for higher energy collision induced dissociation (CID) with a collision energy set to 35 eV and mass resolution to 60,000. The FT AGC target was set to 1e6 and the scan range set to 400-1800 m/z. The MS2 AGC target was 3e4 and dynamic exclusion was enabled for 30 seconds.

Proteomic statistical analysis

For each LC-MS run, the resulting raw data files were searched using Byonic 2.11.0 (Protein Metrics) Swiss-Prot databases. First, containing reference human proteome (2020; 20,626 entries), and again using reference mouse proteome (2020; 17,282 entries). Parameters included trypsin digestion with a maximum of two missed cleavages and precursor mass tolerance of 10 ppm, and 0.5 Da for fragment masses. Fixed cysteine carbamidomethylation and variable methionine oxidation and asparagine deamination were also specified. Peptide identification was filtered to remove hits with > 1% false discovery rate (FDR). Peptides that overlapped in human and mouse searches were removed for a conservative analysis of only human-specific proteins using an in-house R script, for each of the two biological replicates, and three injections per sample. Quantitative values were extracted from MS1 spectra from all identified peptides using an in-house R script based on MSnbase package [85], and abundance changes analyzed using Generic Integration Algorithm. Calculation of statistical weight was performed at spectrum level using WSPP model [86]. Final statistical analysis was performed using student's T-test, considering only proteins having a *p*-value less than 1%. These proteins were analyzed on String network analysis (String-db.org), and Enrichr (https://maayanlab.cloud/Enrichr/).

Statistics

Student's t-test was performed to compare two groups unless otherwise noted. For all, *p*-values of 0.05 or less were considered statistically significant. **** = $P < 0.0001$, *** = $P < 0.005$, ** = $P < 0.01$, * = $P < 0.05$, and n.s. = not significant.

Acknowledgements

This study was supported by the National Institutes of Health/National Cancer Institute (NCI) R01CA244281, US Department of

Defense award HT9425-231-1034, National Institutes of Health/NCI P50CA092131, and the UCLA Jonsson Comprehensive Cancer Center. T.S. is supported by the National Institutes of Health (NIH)/National Cancer Institute (NCI) (R37CA240822, R01CA244281, P50CA092131, R01CA274978 and R01CA-287669) and by the United States Department of Defense (Award Numbers HT9425-23-1-1034 and HT9425-24-1-0396). The content is solely the responsibility of the authors and does not necessarily represent the official views of the Department of Defense. S.L. is supported by the Jonsson Comprehensive Cancer Center Fellowship Award.

Disclosure of conflict of interest

None.

Address correspondence to: Tanya Stoyanova, Department of Molecular and Medical Pharmacology, University of California, Los Angeles, Los Angeles, CA, USA. E-mail: tstoyanova@mednet.ucla.edu

References

[1] Siegel RL, Giaquinto AN and Jemal A. Cancer statistics, 2024. CA Cancer J Clin 2024; 74: 12-49.

[2] Sartor O and de Bono JS. Metastatic prostate cancer. N Engl J Med 2018; 378: 645-657.

[3] Sandhu S, Moore CM, Chiong E, Beltran H, Bristow RG and Williams SG. Prostate cancer. Lancet 2021; 398: 1075-1090.

[4] Abida W, Cyrta J, Heller G, Prandi D, Armenia J, Coleman I, Cieslik M, Benelli M, Robinson D, Van Allen EM, Sboner A, Fedrizzi T, Mosquera JM, Robinson BD, De Sarkar N, Kunju LP, Tomlins S, Wu YM, Nava Rodrigues D, Loda M, Gopalan A, Reuter VE, Pritchard CC, Mateo J, Bianchini D, Miranda S, Carreira S, Rescigno P, Filipenko J, Vinson J, Montgomery RB, Beltran H, Heath EI, Scher HI, Kantoff PW, Taplin ME, Schultz N, deBono JS, Demichelis F, Nelson PS, Rubin MA, Chinnaiyan AM and Sawyers CL. Genomic correlates of clinical outcome in advanced prostate cancer. Proc Natl Acad Sci U S A 2019; 116: 11428-11436.

[5] Adams EJ, Karthaus WR, Hoover E, Liu D, Gruet A, Zhang Z, Cho H, DiLoreto R, Chhangawala S, Liu Y, Watson PA, Davicioni E, Sboner A, Barbieri CE, Bose R, Leslie CS and Sawyers CL. FOXA1 mutations alter pioneering activity, differentiation and prostate cancer phenotypes. Nature 2019; 571: 408-412.

[6] Akamatsu S, Wyatt AW, Lin D, Lysakowski S, Zhang F, Kim S, Tse C, Wang K, Mo F, Haegert A, Brahmbhatt S, Bell R, Adomat H, Kawai Y, Xue H, Dong X, Fazli L, Tsai H, Lotan TL, Kossai M, Mosquera JM, Rubin MA, Beltran H, Zoubeidi A, Wang Y, Gleave ME and Collins CC. The placental gene PEG10 promotes progression of neuroendocrine prostate cancer. Cell Rep 2015; 12: 922-936.

[7] Augspach A, Drake KD, Roma L, Qian E, Lee SR, Clarke D, Kumar S, Jaquet M, Gallon J, Bolis M, Triscott J, Galván JA, Chen Y, Thalmann GN, Kruithof-de Julio M, Theurillat JP, Wuchty S, Gerstein M, Piscuoglio S, Kanadia RN and Rubin MA. Minor intron splicing is critical for survival of lethal prostate cancer. Mol Cell 2023; 83: 1983-2002, e1911.

[8] Baca SC, Takeda DY, Seo JH, Hwang J, Ku SY, Arafeh R, Arnoff T, Agarwal S, Bell C, O'Connor E, Qiu X, Alaiwi SA, Corona RI, Fonseca MAS, Giambartolomei C, Cejas P, Lim K, He M, Sheahan A, Nassar A, Berchuck JE, Brown L, Nguyen HM, Coleman IM, Kaipainen A, De Sarkar N, Nelson PS, Morrissey C, Korthauer K, Pomerantz MM, Ellis L, Pasaniuc B, Lawrenson K, Kelly K, Zoubeidi A, Hahn WC, Beltran H, Long HW, Brown M, Corey E and Freedman ML. Reprogramming of the FOXA1 cistrome in treatment-emergent neuroendocrine prostate cancer. Nat Commun 2021; 12: 1979.

[9] Barbieri CE, Baca SC, Lawrence MS, Demichelis F, Blattner M, Theurillat JP, White TA, Stojanov P, Van Allen E, Stransky N, Nickerson E, Chae SS, Boysen G, Auclair D, Onofrio RC, Park K, Kitabayashi N, MacDonald TY, Sheikh K, Vuong T, Guiducci C, Cibulskis K, Sivachenko A, Carter SL, Saksena G, Voet D, Hussain WM, Ramos AH, Winckler W, Redman MC, Ardlie K, Tewari AK, Mosquera JM, Rupp N, Wild PJ, Moch H, Morrissey C, Nelson PS, Kantoff PW, Gabriel SB, Golub TR, Meyerson M, Lander ES, Getz G, Rubin MA and Garraway LA. Exome sequencing identifies recurrent SPOP, FOXA1 and MED12 mutations in prostate cancer. Nat Genet 2012; 44: 685-689.

[10] Beltran H, Hruszkewycz A, Scher HI, Hildesheim J, Isaacs J, Yu EY, Kelly K, Lin D, Dicker A, Arnold J, Hecht T, Wicha M, Sears R, Rowley D, White R, Gulley JL, Lee J, Diaz Meco M, Small EJ, Shen M, Knudsen K, Goodrich DW, Lotan T, Zoubeidi A, Sawyers CL, Rudin CM, Loda M, Thompson T, Rubin MA, Tawab-Amiri A, Dahut W and Nelson PS. The role of lineage plasticity in prostate cancer therapy resistance. Clin Cancer Res 2019; 25: 6916-6924.

[11] Beltran H, Prandi D, Mosquera JM, Benelli M, Puca L, Cyrta J, Marotz C, Giannopoulou E, Chakravarthi BV, Varambally S, Tomlins SA, Nanus DM, Tagawa ST, Van Allen EM, Elemento O, Sboner A, Garraway LA, Rubin MA and Demichelis F. Divergent clonal evolution of

castration-resistant neuroendocrine prostate cancer. Nat Med 2016; 22: 298-305.

[12] Beltran H, Romanel A, Conteduca V, Casiraghi N, Sigouros M, Franceschini GM, Orlando F, Fedrizzi T, Ku SY, Dann E, Alonso A, Mosquera JM, Sboner A, Xiang J, Elemento O, Nanus DM, Tagawa ST, Benelli M and Demichelis F. Circulating tumor DNA profile recognizes transformation to castration-resistant neuroendocrine prostate cancer. J Clin Invest 2020; 130: 1653-1668.

[13] Bishop JL, Thaper D, Vahid S, Davies A, Ketola K, Kuruma H, Jama R, Nip KM, Angeles A, Johnson F, Wyatt AW, Fazli L, Gleave ME, Lin D, Rubin MA, Collins CC, Wang Y, Beltran H and Zoubeidi A. The master neural transcription factor BRN2 is an androgen receptor-suppressed driver of neuroendocrine differentiation in prostate cancer. Cancer Discov 2017; 7: 54-71.

[14] Bolis M, Bossi D, Vallerga A, Ceserani V, Cavalli M, Impellizzieri D, Di Rito L, Zoni E, Mosole S, Elia AR, Rinaldi A, Pereira Mestre R, D'Antonio E, Ferrari M, Stoffel F, Jermini F, Gillessen S, Bubendorf L, Schraml P, Calcinotto A, Corey E, Moch H, Spahn M, Thalmann G, Kruithof-de Julio M, Rubin MA and Theurillat JP. Dynamic prostate cancer transcriptome analysis delineates the trajectory to disease progression. Nat Commun 2021; 12: 7033.

[15] Brady NJ, Bagadion AM, Singh R, Conteduca V, Van Emmenis L, Arceci E, Pakula H, Carelli R, Khani F, Bakht M, Sigouros M, Bareja R, Sboner A, Elemento O, Tagawa S, Nanus DM, Loda M, Beltran H, Robinson B and Rickman DS. Temporal evolution of cellular heterogeneity during the progression to advanced AR-negative prostate cancer. Nat Commun 2021; 12: 3372.

[16] Butler W and Huang J. Neuroendocrine cells of the prostate: histology, biological functions, and molecular mechanisms. Precis Clin Med 2021; 4: 25-34.

[17] Cejas P, Xie Y, Font-Tello A, Lim K, Syamala S, Qiu X, Tewari AK, Shah N, Nguyen HM, Patel RA, Brown L, Coleman I, Hackeng WM, Brosens L, Dreijerink KMA, Ellis L, Alaiwi SA, Seo JH, Baca S, Beltran H, Khani F, Pomerantz M, Dall'Agnese A, Crowdis J, Van Allen EM, Bellmunt J, Morrisey C, Nelson PS, DeCaprio J, Farago A, Dyson N, Drapkin B, Liu XS, Freedman M, Haffner MC, Corey E, Brown M and Long HW. Subtype heterogeneity and epigenetic convergence in neuroendocrine prostate cancer. Nat Commun 2021; 12: 5775.

[18] Dardenne E, Beltran H, Benelli M, Gayvert K, Berger A, Puca L, Cyrta J, Sboner A, Noorzad Z, MacDonald T, Cheung C, Yuen KS, Gao D, Chen Y, Eilers M, Mosquera JM, Robinson BD, Elemento O, Rubin MA, Demichelis F and Rickman DS. N-Myc induces an EZH2-mediated transcriptional program driving neuroendocrine prostate cancer. Cancer Cell 2016; 30: 563-577.

[19] Davies A, Nouruzi S, Ganguli D, Namekawa T, Thaper D, Linder S, Karaoğlanoğlu F, Omur ME, Kim S, Kobelev M, Kumar S, Sivak O, Bostock C, Bishop J, Hoogstraat M, Talal A, Stelloo S, van der Poel H, Bergman AM, Ahmed M, Fazli L, Huang H, Tilley W, Goodrich D, Feng FY, Gleave M, He HH, Hach F, Zwart W, Beltran H, Selth L and Zoubeidi A. An androgen receptor switch underlies lineage infidelity in treatment-resistant prostate cancer. Nat Cell Biol 2021; 23: 1023-1034.

[20] Davies AH, Beltran H and Zoubeidi A. Cellular plasticity and the neuroendocrine phenotype in prostate cancer. Nat Rev Urol 2018; 15: 271-286.

[21] Dehm SM, Schmidt LJ, Heemers HV, Vessella RL and Tindall DJ. Splicing of a novel androgen receptor exon generates a constitutively active androgen receptor that mediates prostate cancer therapy resistance. Cancer Res 2008; 68: 5469-5477.

[22] Fraser M, Sabelnykova VY, Yamaguchi TN, Heisler LE, Livingstone J, Huang V, Shiah YJ, Yousif F, Lin X, Masella AP, Fox NS, Xie M, Prokopec SD, Berlin A, Lalonde E, Ahmed M, Trudel D, Luo X, Beck TA, Meng A, Zhang J, D'Costa A, Denroche RE, Kong H, Espiritu SM, Chua ML, Wong A, Chong T, Sam M, Johns J, Timms L, Buchner NB, Orain M, Picard V, Hovington H, Murison A, Kron K, Harding NJ, P'ng C, Houlahan KE, Chu KC, Lo B, Nguyen F, Li CH, Sun RX, de Borja R, Cooper CI, Hopkins JF, Govind SK, Fung C, Waggott D, Green J, Haider S, Chan-Seng-Yue MA, Jung E, Wang Z, Bergeron A, Dal Pra A, Lacombe L, Collins CC, Sahinalp C, Lupien M, Fleshner NE, He HH, Fradet Y, Tetu B, van der Kwast T, McPherson JD, Bristow RG and Boutros PC. Genomic hallmarks of localized, non-indolent prostate cancer. Nature 2017; 541: 359-364.

[23] Grasso CS, Wu YM, Robinson DR, Cao X, Dhanasekaran SM, Khan AP, Quist MJ, Jing X, Lonigro RJ, Brenner JC, Asangani IA, Ateeq B, Chun SY, Siddiqui J, Sam L, Anstett M, Mehra R, Prensner JR, Palanisamy N, Ryslik GA, Vandin F, Raphael BJ, Kunju LP, Rhodes DR, Pienta KJ, Chinnaiyan AM and Tomlins SA. The mutational landscape of lethal castration-resistant prostate cancer. Nature 2012; 487: 239-243.

[24] Ku SY, Rosario S, Wang Y, Mu P, Seshadri M, Goodrich ZW, Goodrich MM, Labbé DP, Gomez EC, Wang J, Long HW, Xu B, Brown M, Loda M,

Sawyers CL, Ellis L and Goodrich DW. Rb1 and Trp53 cooperate to suppress prostate cancer lineage plasticity, metastasis, and antiandrogen resistance. Science 2017; 355: 78-83.

[25] Lee JK, Phillips JW, Smith BA, Park JW, Stoyanova T, McCaffrey EF, Baertsch R, Sokolov A, Meyerowitz JG, Mathis C, Cheng D, Stuart JM, Shokat KM, Gustafson WC, Huang J and Witte ON. N-Myc drives neuroendocrine prostate cancer initiated from human prostate epithelial cells. Cancer Cell 2016; 29: 536-547.

[26] Li Y, Hwang TH, Oseth LA, Hauge A, Vessella RL, Schmechel SC, Hirsch B, Beckman KB, Silverstein KA and Dehm SM. AR intragenic deletions linked to androgen receptor splice variant expression and activity in models of prostate cancer progression. Oncogene 2012; 31: 4759-4767.

[27] Li Y, Yang R, Henzler CM, Ho Y, Passow C, Auch B, Carreira S, Nava Rodrigues D, Bertan C, Hwang TH, Quigley DA, Dang HX, Morrissey C, Fraser M, Plymate SR, Maher CA, Feng FY, de Bono JS and Dehm SM. Diverse AR gene rearrangements mediate resistance to androgen receptor inhibitors in metastatic prostate cancer. Clin Cancer Res 2020; 26: 1965-1976.

[28] Liu S, Alabi BR, Yin Q and Stoyanova T. Molecular mechanisms underlying the development of neuroendocrine prostate cancer. Semin Cancer Biol 2022; 86: 57-68.

[29] Lundberg A, Zhang M, Aggarwal R, Li H, Zhang L, Foye A, Sjöström M, Chou J, Chang K, Moreno-Rodriguez T, Shrestha R, Baskin A, Zhu X, Weinstein AS, Younger N, Alumkal JJ, Beer TM, Chi KN, Evans CP, Gleave M, Lara PN, Reiter RE, Rettig MB, Witte ON, Wyatt AW, Feng FY, Small EJ and Quigley DA. The genomic and epigenomic landscape of double-negative metastatic prostate cancer. Cancer Res 2023; 83: 2763-2774.

[30] Lupien M, Eeckhoute J, Meyer CA, Wang Q, Zhang Y, Li W, Carroll JS, Liu XS and Brown M. FoxA1 translates epigenetic signatures into enhancer-driven lineage-specific transcription. Cell 2008; 132: 958-970.

[31] Mu P, Zhang Z, Benelli M, Karthaus WR, Hoover E, Chen CC, Wongvipat J, Ku SY, Gao D, Cao Z, Shah N, Adams EJ, Abida W, Watson PA, Prandi D, Huang CH, de Stanchina E, Lowe SW, Ellis L, Beltran H, Rubin MA, Goodrich DW, Demichelis F and Sawyers CL. SOX2 promotes lineage plasticity and antiandrogen resistance in TP53- and RB1-deficient prostate cancer. Science 2017; 355: 84-88.

[32] Nava Rodrigues D, Casiraghi N, Romanel A, Crespo M, Miranda S, Rescigno P, Figueiredo I, Riisnaes R, Carreira S, Sumanasuriya S, Gasperini P, Sharp A, Mateo J, Makay A, McNair C, Schiewer M, Knudsen K, Boysen G, Demichelis F and de Bono JS. RB1 heterogeneity in advanced metastatic castration-resistant prostate cancer. Clin Cancer Res 2019; 25: 687-697.

[33] Nouruzi S, Ganguli D, Tabrizian N, Kobelev M, Sivak O, Namekawa T, Thaper D, Baca SC, Freedman ML, Aguda A, Davies A and Zoubeidi A. ASCL1 activates neuronal stem cell-like lineage programming through remodeling of the chromatin landscape in prostate cancer. Nat Commun 2022; 13: 2282.

[34] Nyquist MD, Corella A, Coleman I, De Sarkar N, Kaipainen A, Ha G, Gulati R, Ang L, Chatterjee P, Lucas J, Pritchard C, Risbridger G, Isaacs J, Montgomery B, Morrissey C, Corey E and Nelson PS. Combined TP53 and RB1 loss promotes prostate cancer resistance to a spectrum of therapeutics and confers vulnerability to replication stress. Cell Rep 2020; 31: 107669.

[35] Park JW, Lee JK, Sheu KM, Wang L, Balanis NG, Nguyen K, Smith BA, Cheng C, Tsai BL, Cheng D, Huang J, Kurdistani SK, Graeber TG and Witte ON. Reprogramming normal human epithelial tissues to a common, lethal neuroendocrine cancer lineage. Science 2018; 362: 91-95.

[36] Quigley DA, Dang HX, Zhao SG, Lloyd P, Aggarwal R, Alumkal JJ, Foye A, Kothari V, Perry MD, Bailey AM, Playdle D, Barnard TJ, Zhang L, Zhang J, Youngren JF, Cieslik MP, Parolia A, Beer TM, Thomas G, Chi KN, Gleave M, Lack NA, Zoubeidi A, Reiter RE, Rettig MB, Witte O, Ryan CJ, Fong L, Kim W, Friedlander T, Chou J, Li H, Das R, Li H, Moussavi-Baygi R, Goodarzi H, Gilbert LA, Lara PN Jr, Evans CP, Goldstein TC, Stuart JM, Tomlins SA, Spratt DE, Cheetham RK, Cheng DT, Farh K, Gehring JS, Hakenberg J, Liao A, Febbo PG, Shon J, Sickler B, Batzoglou S, Knudsen KE, He HH, Huang J, Wyatt AW, Dehm SM, Ashworth A, Chinnaiyan AM, Maher CA, Small EJ and Feng FY. Genomic hallmarks and structural variation in metastatic prostate cancer. Cell 2018; 174: 758-769, e759.

[37] Robinson D, Van Allen EM, Wu YM, Schultz N, Lonigro RJ, Mosquera JM, Montgomery B, Taplin ME, Pritchard CC, Attard G, Beltran H, Abida W, Bradley RK, Vinson J, Cao X, Vats P, Kunju LP, Hussain M, Feng FY, Tomlins SA, Cooney KA, Smith DC, Brennan C, Siddiqui J, Mehra R, Chen Y, Rathkopf DE, Morris MJ, Solomon SB, Durack JC, Reuter VE, Gopalan A, Gao J, Loda M, Lis RT, Bowden M, Balk SP, Gaviola G, Sougnez C, Gupta M, Yu EY, Mostaghel EA, Cheng HH, Mulcahy H, True LD, Plymate SR, Dvinge H, Ferraldeschi R, Flohr P, Miranda S, Zafeiriou Z, Tunariu N, Mateo J, Perez-Lopez R, Demichelis F, Robinson BD, Schiffman M, Nanus DM, Tagawa ST, Sigaras

A, Eng KW, Elemento O, Sboner A, Heath EI, Scher HI, Pienta KJ, Kantoff P, de Bono JS, Rubin MA, Nelson PS, Garraway LA, Sawyers CL and Chinnaiyan AM. Integrative clinical genomics of advanced prostate cancer. Cell 2015; 161: 1215-1228.

[38] Rotinen M, You S, Yang J, Coetzee SG, Reis-Sobreiro M, Huang WC, Huang F, Pan X, Yáñez A, Hazelett DJ, Chu CY, Steadman K, Morrissey CM, Nelson PS, Corey E, Chung LWK, Freedland SJ, Di Vizio D, Garraway IP, Murali R, Knudsen BS and Freeman MR. ONECUT2 is a targetable master regulator of lethal prostate cancer that suppresses the androgen axis. Nat Med 2018; 24: 1887-1898.

[39] Valentin Lopez JC, Lange CA and Dehm SM. Androgen receptor and estrogen receptor variants in prostate and breast cancers. J Steroid Biochem Mol Biol 2024; 241: 106522.

[40] Vlachostergios PJ, Puca L and Beltran H. Emerging variants of castration-resistant prostate cancer. Curr Oncol Rep 2017; 19: 32.

[41] Wang Y, Wang Y, Ci X, Choi SYC, Crea F, Lin D and Wang Y. Molecular events in neuroendocrine prostate cancer development. Nat Rev Urol 2021; 18: 581-596.

[42] Zhao SG, Chen WS, Li H, Foye A, Zhang M, Sjöström M, Aggarwal R, Playdle D, Liao A, Alumkal JJ, Das R, Chou J, Hua JT, Barnard TJ, Bailey AM, Chow ED, Perry MD, Dang HX, Yang R, Moussavi-Baygi R, Zhang L, Alshalalfa M, Laura Chang S, Houlahan KE, Shiah YJ, Beer TM, Thomas G, Chi KN, Gleave M, Zoubeidi A, Reiter RE, Rettig MB, Witte O, Yvonne Kim M, Fong L, Spratt DE, Morgan TM, Bose R, Huang FW, Li H, Chesner L, Shenoy T, Goodarzi H, Asangani IA, Sandhu S, Lang JM, Mahajan NP, Lara PN, Evans CP, Febbo P, Batzoglou S, Knudsen KE, He HH, Huang J, Zwart W, Costello JF, Luo J, Tomlins SA, Wyatt AW, Dehm SM, Ashworth A, Gilbert LA, Boutros PC, Farh K, Chinnaiyan AM, Maher CA, Small EJ, Quigley DA and Feng FY. The DNA methylation landscape of advanced prostate cancer. Nat Genet 2020; 52: 778-789.

[43] Zivanovic A, Miller JT, Munro SA, Knutson TP, Li Y, Passow CN, Simonaitis P, Lynch M, Oseth L, Zhao SG, Feng FY, Wikström P, Corey E, Morrissey C, Henzler C, Raphael BJ and Dehm SM. Co-evolution of AR gene copy number and structural complexity in endocrine therapy resistant prostate cancer. NAR Cancer 2023; 5: zcad045.

[44] Cheng Q, Butler W, Zhou Y, Zhang H, Tang L, Perkinson K, Chen X, Jiang XS, McCall SJ, Inman BA and Huang J. Pre-existing castration-resistant prostate cancer-like cells in primary prostate cancer promote resistance to hormonal therapy. Eur Urol 2022; 81: 446-455.

[45] Faubert B, Solmonson A and DeBerardinis RJ. Metabolic reprogramming and cancer progression. Science 2020; 368: eaaw5473.

[46] Watson PA, Arora VK and Sawyers CL. Emerging mechanisms of resistance to androgen receptor inhibitors in prostate cancer. Nat Rev Cancer 2015; 15: 701-711.

[47] Quintanal-Villalonga A, Chan JM, Yu HA, Pe'er D, Sawyers CL, Sen T and Rudin CM. Lineage plasticity in cancer: a shared pathway of therapeutic resistance. Nat Rev Clin Oncol 2020; 17: 360-371.

[48] Schaeffer EM, Srinivas S, Adra N, An Y, Barocas D, Bitting R, Bryce A, Chapin B, Cheng HH, D'Amico AV, Desai N, Dorff T, Eastham JA, Farrington TA, Gao X, Gupta S, Guzzo T, Ippolito JE, Kuettel MR, Lang JM, Lotan T, McKay RR, Morgan T, Netto G, Pow-Sang JM, Reiter R, Roach M, Robin T, Rosenfeld S, Shabsigh A, Spratt D, Teply BA, Tward J, Valicenti R, Wong JK, Shead DA, Snedeker J and Freedman-Cass DA. Prostate cancer, version 4.2023, NCCN Clinical Practice Guidelines in Oncology. J Natl Compr Canc Netw 2023; 21: 1067-1096.

[49] Wang G, Zhao D, Spring DJ and DePinho RA. Genetics and biology of prostate cancer. Genes Dev 2018; 32: 1105-1140.

[50] Davis ID, Martin AJ, Stockler MR, Begbie S, Chi KN, Chowdhury S, Coskinas X, Frydenberg M, Hague WE, Horvath LG, Joshua AM, Lawrence NJ, Marx G, McCaffrey J, McDermott R, McJannett M, North SA, Parnis F, Parulekar W, Pook DW, Reaume MN, Sandhu SK, Tan A, Tan TH, Thomson A, Tu E, Vera-Badillo F, Williams SG, Yip S, Zhang AY, Zielinski RR and Sweeney CJ; ENZAMET Trial Investigators and the Australian and New Zealand Urogenital and Prostate Cancer Trials Group. Enzalutamide with standard first-line therapy in metastatic prostate cancer. N Engl J Med 2019; 381: 121-131.

[51] Yamada Y and Beltran H. The treatment landscape of metastatic prostate cancer. Cancer Lett 2021; 519: 20-29.

[52] Desai K, McManus JM and Sharifi N. Hormonal therapy for prostate cancer. Endocr Rev 2021; 42: 354-373.

[53] Westaby D, Viscuse PV, Ravilla R, de la Maza MLDF, Hahn A, Sharp A, de Bono J, Aparicio A and Fleming MT. Beyond the androgen receptor: the sequence, the mutants, and new avengers in the treatment of castrate-resistant metastatic prostate cancer. Am Soc Clin Oncol Educ Book 2021; 41: e190-e202.

[54] Labrecque MP, Coleman IM, Brown LG, True LD, Kollath L, Lakely B, Nguyen HM, Yang YC, da Costa RMG, Kaipainen A, Coleman R, Higano CS, Yu EY, Cheng HH, Mostaghel EA, Montgomery B, Schweizer MT, Hsieh AC, Lin DW, Corey E, Nelson PS and Morrissey C.

Molecular profiling stratifies diverse phenotypes of treatment-refractory metastatic castration-resistant prostate cancer. J Clin Invest 2019; 129: 4492-4505.
[55] Vellky JE and Ricke WA. Development and prevalence of castration-resistant prostate cancer subtypes. Neoplasia 2020; 22: 566-575.
[56] Brennen WN, Zhu Y, Coleman IM, Dalrymple SL, Antony L, Patel RA, Hanratty B, Chikarmane R, Meeker AK, Zheng SL, Hooper JE, Luo J, De Marzo AM, Corey E, Xu J, Yegnasubramanian S, Haffner MC, Nelson PS, Nelson WG, Isaacs WB and Isaacs JT. Resistance to androgen receptor signaling inhibition does not necessitate development of neuroendocrine prostate cancer. JCI Insight 2021; 6: e146827.
[57] Bluemn EG, Coleman IM, Lucas JM, Coleman RT, Hernandez-Lopez S, Tharakan R, Bianchi-Frias D, Dumpit RF, Kaipainen A, Corella AN, Yang YC, Nyquist MD, Mostaghel E, Hsieh AC, Zhang X, Corey E, Brown LG, Nguyen HM, Pienta K, Ittmann M, Schweizer M, True LD, Wise D, Rennie PS, Vessella RL, Morrissey C and Nelson PS. Androgen receptor pathway-independent prostate cancer is sustained through FGF signaling. Cancer Cell 2017; 32: 474-489, e476.
[58] Cheng S, Li L, Yeh Y, Shi Y, Franco O, Corey E and Yu X. Unveiling novel double-negative prostate cancer subtypes through single-cell RNA sequencing analysis. NPJ Precis Oncol 2024; 8: 171.
[59] Berchuck JE, Viscuse PV, Beltran H and Aparicio A. Clinical considerations for the management of androgen indifferent prostate cancer. Prostate Cancer Prostatic Dis 2021; 24: 623-637.
[60] Shrestha R, Chesner LN, Zhang M, Zhou S, Foye A, Lundberg A, Weinstein AS, Sjöström M, Zhu X, Moreno-Rodriguez T, Li H; SU2C/PCF West Coast Prostate Cancer Dream Team; Alumkal JJ, Aggarwal R, Small EJ, Lupien M, Quigley DA and Feng FY. An atlas of accessible chromatin in advanced prostate cancer reveals the epigenetic evolution during tumor progression. Cancer Res 2024; 84: 3086-3100.
[61] Wise DR, Schneider JA, Armenia J, Febles VA, McLaughlin B, Brennan R, Thoren KL, Abida W, Sfanos KS, De Marzo AM, Yegnasubramanian S, Fox JJ, Haas M, Heath H, Kagey MH, Newman W, Sirard CA, Fleisher M, Morris MJ, Chen Y, Larson SM, Haffner MC, Nelson PS, Schultz N, Garabedian MJ, Scher HI, Logan SK and Sawyers CL; International SU2C/PCF Prostate Cancer Dream Team. Dickkopf-1 can lead to immune evasion in metastatic castration-resistant prostate cancer. JCO Precis Oncol 2020; 4: PO.20.00097.
[62] Tang H, Gupta A, Morrisroe SA, Bao C, Schwantes-An TH, Gupta G, Liang S, Sun Y, Chu A, Luo A, Ramamoorthi Elangovan V, Sangam S, Shi Y, Naidu SR, Jheng JR, Ciftci-Yilmaz S, Warfel NA, Hecker L, Mitra S, Coleman AW, Lutz KA, Pauciulo MW, Lai YC, Javaheri A, Dharmakumar R, Wu WH, Flaherty DP, Karnes JH, Breuils-Bonnet S, Boucherat O, Bonnet S, Yuan JX, Jacobson JR, Duarte JD, Nichols WC, Garcia JGN and Desai AA. Deficiency of the deubiquitinase UCHL1 attenuates pulmonary arterial hypertension. Circulation 2024; 150: 302-316.
[63] Bi HL, Zhang XL, Zhang YL, Xie X, Xia YL, Du J and Li HH. The deubiquitinase UCHL1 regulates cardiac hypertrophy by stabilizing epidermal growth factor receptor. Sci Adv 2020; 6: eaax4826.
[64] Mi Z and Graham SH. Role of UCHL1 in the pathogenesis of neurodegenerative diseases and brain injury. Ageing Res Rev 2023; 86: 101856.
[65] Rentsendorj A, Raedschelders K, Fuchs DT, Sheyn J, Vaibhav V, Porritt RA, Shi H, Dagvadorj J, de Freitas Germano J, Koronyo Y, Arditi M, Black KL, Gaire BP, Van Eyk JE and Koronyo-Hamaoui M. Osteopontin depletion in macrophages perturbs proteostasis via regulating UCHL1-UPS axis and mitochondria-mediated apoptosis. Front Immunol 2023; 14: 1155935.
[66] Ding X, Gu Y, Jin M, Guo X, Xue S, Tan C, Huang J, Yang W, Xue M, Zhou Q, Wang W and Zhang Y. The deubiquitinating enzyme UCHL1 promotes resistance to pemetrexed in non-small cell lung cancer by upregulating thymidylate synthase. Theranostics 2020; 10: 6048-6060.
[67] Goto Y, Zeng L, Yeom CJ, Zhu Y, Morinibu A, Shinomiya K, Kobayashi M, Hirota K, Itasaka S, Yoshimura M, Tanimoto K, Torii M, Sowa T, Menju T, Sonobe M, Kakeya H, Toi M, Date H, Hammond EM, Hiraoka M and Harada H. UCHL1 provides diagnostic and antimetastatic strategies due to its deubiquitinating effect on HIF-1alpha. Nat Commun 2015; 6: 6153.
[68] Jin C, Yu W, Lou X, Zhou F, Han X, Zhao N and Lin B. UCHL1 is a putative tumor suppressor in ovarian cancer cells and contributes to cisplatin resistance. J Cancer 2013; 4: 662-670.
[69] Li J, Liang Y, Zhou S, Chen J and Wu C. UCHL1 contributes to insensitivity to endocrine therapy in triple-negative breast cancer by deubiquitinating and stabilizing KLF5. Breast Cancer Res 2024; 26: 44.
[70] Liu S, Chai T, Garcia-Marques F, Yin Q, Hsu EC, Shen M, Shaw Toland AM, Bermudez A, Hartono AB, Massey CF, Lee CS, Zheng L, Baron M, Denning CJ, Aslan M, Nguyen HM, Nolley R, Zoubeidi A, Das M, Kunder CA, Howitt BE, Soh HT, Weissman IL, Liss MA, Chin AI, Brooks JD, Corey E, Pitteri SJ, Huang J and Stoyanova T. UCHL1 is a potential molecular

indicator and therapeutic target for neuroendocrine carcinomas. Cell Rep Med 2024; 5: 101381.
[71] Ummanni R, Jost E, Braig M, Lohmann F, Mundt F, Barett C, Schlomm T, Sauter G, Senff T, Bokemeyer C, Sültmann H, Meyer-Schwesinger C, Brümmendorf TH and Balabanov S. Ubiquitin carboxyl-terminal hydrolase 1 (UCHL1) is a potential tumour suppressor in prostate cancer and is frequently silenced by promoter methylation. Mol Cancer 2011; 10: 129.
[72] Kumar A, Coleman I, Morrissey C, Zhang X, True LD, Gulati R, Etzioni R, Bolouri H, Montgomery B, White T, Lucas JM, Brown LG, Dumpit RF, DeSarkar N, Higano C, Yu EY, Coleman R, Schultz N, Fang M, Lange PH, Shendure J, Vessella RL and Nelson PS. Substantial interindividual and limited intraindividual genomic diversity among tumors from men with metastatic prostate cancer. Nat Med 2016; 22: 369-378.
[73] Taylor BS, Schultz N, Hieronymus H, Gopalan A, Xiao Y, Carver BS, Arora VK, Kaushik P, Cerami E, Reva B, Antipin Y, Mitsiades N, Landers T, Dolgalev I, Major JE, Wilson M, Socci ND, Lash AE, Heguy A, Eastham JA, Scher HI, Reuter VE, Scardino PT, Sander C, Sawyers CL and Gerald WL. Integrative genomic profiling of human prostate cancer. Cancer Cell 2010; 18: 11-22.
[74] Hsu EC, Rice MA, Bermudez A, Marques FJG, Aslan M, Liu S, Ghoochani A, Zhang CA, Chen YS, Zlitni A, Kumar S, Nolley R, Habte F, Shen M, Koul K, Peehl DM, Zoubeidi A, Gambhir SS, Kunder CA, Pitteri SJ, Brooks JD and Stoyanova T. Trop2 is a driver of metastatic prostate cancer with neuroendocrine phenotype via PARP1. Proc Natl Acad Sci U S A 2020; 117: 2032-2042.
[75] Liu S, Hsu EC, Shen M, Aslan M and Stoyanova T. Metastasis model to test the role of notch signaling in prostate cancer. Methods Mol Biol 2022; 2472: 221-233.
[76] Nijman SM, Luna-Vargas MP, Velds A, Brummelkamp TR, Dirac AM, Sixma TK and Bernards R. A genomic and functional inventory of deubiquitinating enzymes. Cell 2005; 123: 773-786.
[77] Larsen CN, Price JS and Wilkinson KD. Substrate binding and catalysis by ubiquitin C-terminal hydrolases: identification of two active site residues. Biochemistry 1996; 35: 6735-6744.
[78] Shen MM. A positive step toward understanding double-negative metastatic prostate cancer. Cancer Cell 2019; 36: 117-119.
[79] Labrecque MP, Brown LG, Coleman IM, Nguyen HM, Dalrymple S, Brennen WN, Isaacs JT, Li D, Lakely B, DeLucia DC, Lee JK, Schweizer MT, Lin DW, Corey E, Nelson PS and Morrissey C. Targeting the fibroblast growth factor pathway in molecular subtypes of castration-resistant prostate cancer. Prostate 2024; 84: 100-110.
[80] Su W, Han HH, Wang Y, Zhang B, Zhou B, Cheng Y, Rumandla A, Gurrapu S, Chakraborty G, Su J, Yang G, Liang X, Wang G, Rosen N, Scher HI, Ouerfelli O and Giancotti FG. The polycomb repressor complex 1 drives double-negative prostate cancer metastasis by coordinating stemness and immune suppression. Cancer Cell 2019; 36: 139-155, e110.
[81] Rodriguez Y, Unno K, Truica MI, Chalmers ZR, Yoo YA, Vatapalli R, Sagar V, Yu J, Lysy B, Hussain M, Han H and Abdulkadir SA. A genome-wide CRISPR activation screen identifies PRRX2 as a regulator of enzalutamide resistance in prostate cancer. Cancer Res 2022; 82: 2110-2123.
[82] Hussain S, Bedekovics T, Liu Q, Hu W, Jeon H, Johnson SH, Vasmatzis G, May DG, Roux KJ and Galardy PJ. UCH-L1 bypasses mTOR to promote protein biosynthesis and is required for MYC-driven lymphomagenesis in mice. Blood 2018; 132: 2564-2574.
[83] Hussain S, Foreman O, Perkins SL, Witzig TE, Miles RR, van Deursen J and Galardy PJ. The de-ubiquitinase UCH-L1 is an oncogene that drives the development of lymphoma in vivo by deregulating PHLPP1 and Akt signaling. Leukemia 2010; 24: 1641-1655.
[84] Panyain N, Godinat A, Lanyon-Hogg T, Lachiondo-Ortega S, Will EJ, Soudy C, Mondal M, Mason K, Elkhalifa S, Smith LM, Harrigan JA and Tate EW. Discovery of a potent and selective covalent inhibitor and activity-based probe for the Deubiquitylating enzyme UCHL1, with antifibrotic activity. J Am Chem Soc 2020; 142: 12020-12026.
[85] Gatto L and Lilley KS. MSnbase-an R/Bioconductor package for isobaric tagged mass spectrometry data visualization, processing and quantitation. Bioinformatics 2012; 28: 288-289.
[86] Navarro P, Trevisan-Herraz M, Bonzon-Kulichenko E, Núñez E, Martínez-Acedo P, Pérez-Hernández D, Jorge I, Mesa R, Calvo E, Carrascal M, Hernáez ML, García F, Bárcena JA, Ashman K, Abian J, Gil C, Redondo JM and Vázquez J. General statistical framework for quantitative proteomics by stable isotope labeling. J Proteome Res 2014; 13: 1234-1247.

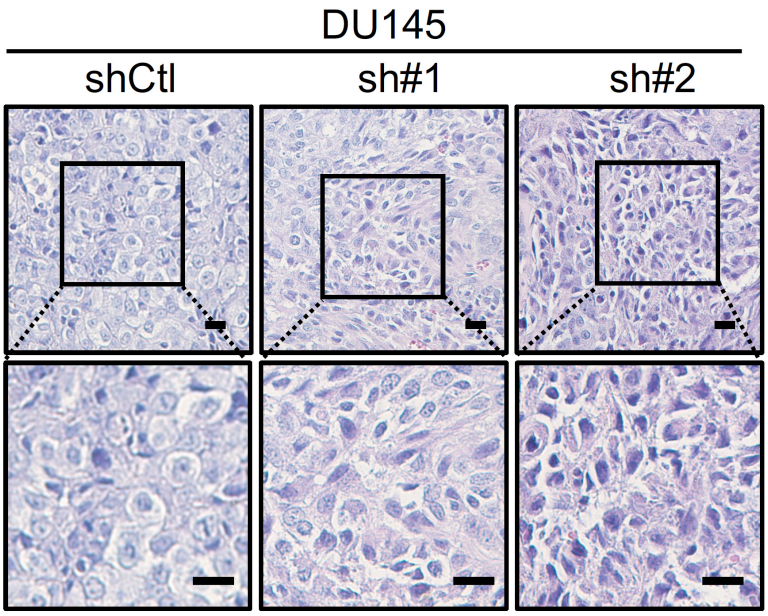

Supplementary Figure 1. Histology of UCH-L1 knockdown in DU-145 xenografts. H.E staining of DU145-shCtl, DU145-shUCH-L1 #1, and DU145-shUCH-L1 #2 xenografts. Scale bars = 20 microns.